Z. Kristallogr. Suppl. **27** (2008) 263-271 / **DOI** 10.1524/zksu.2008.0033
© by Oldenbourg Wissenschaftsverlag, München

Profiling of fibre texture gradients in thin films by anomalous X-ray diffraction

M. Birkholz[1,*], N. Darowski[2], I. Zizak[3]

[1] IHP, Im Technologiepark 25, 15236 Frankfurt (Oder), Germany
[2] Hahn-Meitner-Institut Berlin, Glienicker Str. 100, 14109 Berlin, Germany
[3] Bessy, Albert-Einstein-Str. 15, 12489 Berlin, Germany
[*] birkholz@ihp-microelectronics.com

Keywords: X-ray diffraction, texture, thin films, texture gradient

Abstract. Anomalous X-ray diffraction is applied to the quantitative determination of fiber texture gradients. Use is made of a theoretical model, in which crystallographic texture is described by an order parameter n and the depth dependent $n(z)$ is assumed to follow a linear behavior (M. Birkholz, 2007, *J. Appl. Cryst.*, **40**, 735). The presented method is based on the extension of kinematic diffraction under inclusion of an inhomogeneous texture and relies on the profiling of different layer depths by tuning the wavelength in the neighborhood of an elemental absorption edge. As an example, thin ZnO:Al layers are investigated and large fiber texture gradients dn/dz between 0.03 and 0.3 m.r.d. nm^{-1} (multiples of a random distribution per nanometer) are revealed to occur in these samples. The approach is concluded to be well suited for the study of microstructure evolution as often observed during the growth of thin films.

1. Introduction

Polycrystalline thin films with thicknesses between some nm and some 100 µm play an important role in modern physics and technology. Many of those layer systems are deposited in vacuum-based processes at growth rates between 10^{-1} to 10^{2} nm s^{-1} and, thereby, develop characteristic microstructures that are accounted for by the ratio of deposition over melting temperature as described in structure zone models [1-3]. Next to their technological significance polycrystalline layers are of fundamental interest to condensed matter physics, since they exhibit remarkable growth phenomena. For example, various microstructure parameters often show pronounced gradients such that the crystallite size, residual stress or the crystallographic orientation may increase with increasing thickness. Particularly the distribution of crystallographic orientation or texture represents an interesting order phenomenon; with the preferred crystallographic direction $\langle HKL \rangle$ typically being rotationally symmetric around the substrate normal and thus being denoted as fiber texture or layer texture.
Since many material properties decisively depend on the orientation distribution function of the polycrystalline grain ensemble [4,5], texture and texture gradients are a highly relevant issue for structure-property relations of advanced materials [6,7] and, in particular, of thin films [8]. For instance, in wurtzite-structured ZnO or AlN layers the crystallites have to align their crystallographic c axis along the substrate normal to enable the intended application in

surface acoustic wave devices. Various texture investigations have been performed for elemental metals [9-11], silicon [12-15], TiN [16-26], ZnO [27-30], high-T_c superconducting and dielectric oxides [31, 32] to mention only a small selection of thin film studies. Most of the experiments were performed by X-ray diffraction (XRD) procedures. Although the usage of X-rays advantageously is a non-destructive technique, the experimental determination of texture gradients from an XRD pattern is not straightforward. In most cases a sample series of varying thickness has to be prepared [10, 12, 19, 26, 29, 30, 32] or investigations have to be performed *in-situ* at synchrotron radiation beam lines [25]. Owing to these limitations, only few texture gradients have been determined in a full quantitative manner so far, which contrasts remarkably to their significance for thin film growth.

Besides the lack of experimental data various theoretical models have been developed. The surface energy minimization approach that explains an evolving $\langle HKL \rangle$ fiber by the lowest energy of (HKL) surfaces has found broad dissemination [18, 27, 28]. In an alternative approach van der Drift argued that the difference in crystallographic growth velocities v_{hkl} causes the selection of the fastest growing direction [33]. Other models addressed the competition between surface energy and strain energy elastically stored in the film volume [16, 17] or the effects of impinging low-energy ion currents [11, 20, 24, 31, 34, 35].

From an experimental point of view interesting results on texture developments were obtained recently by Schell et al., who showed that the $\langle 111 \rangle$ fiber texture in magnetron-sputtered TiN layers evolves through a crossover from a $\langle 200 \rangle$ texture in a post-deposition process [25]. Accordingly, effects of dynamic recrystallization play a more important role at low homologous temperatures ($T_h = T_{dep}/T_{melt}$) than has been assumed so far. Also van der Drift's model received experimental confirmation when it was shown for the first time that a direct consequence of the model, which is the simultaneous increase of fiber texture and deposition rate with deposition time, is in fact observed in Al-doped ZnO layers [30]. Nevertheless, more quantitative results on fiber texture developments are required to improve our understanding of the processes that occur during film growth.

In this work, an X-ray diffraction technique will be introduced by which fiber texture gradients of polycrystalline layers can be determined via probing the sample at different depths. Use will be made of the strong variation of X-ray absorption close to the absorption edge of one of the constituting elements and thereby from the variation of average information depth. Samples of ZnO:Al layers with a pronounced $\langle 00L \rangle$ fiber texture will serve as example systems for demonstrating the technique. X-ray energies were accordingly chosen to lie below and above the Zn K edge of 9.67 keV.

2. Profiling by anomalous diffraction

X-ray diffraction experiments in reflection geometry yield structural information from scattering volumes that are restricted by the penetration depth of the radiation. The latter scales with the inverse linear attenuation coefficient $1/\mu$ that depends on the material exposed and on the wavelength λ of the radiation. Due to the exponential damping of the incoming beam different depths contribute to the diffraction pattern with different intensities. Except for grazing-incidence configurations, the illuminated sample volume in thin film XRD typically encompasses the full depth t of the layer [8, 21]. Fiber textures with the fiber axis parallel to the substrate normal $\boldsymbol{s}_3$ may be determined by measuring Bragg peak intensities I_{HKL} or I_H in a symmetrical configuration at scattering angles 2θ under a set of tilt angles ψ that account

for the inclination of the scattering vector $\boldsymbol{Q}$ with respect to $\boldsymbol{s}_3$, see figure1(a). The measurement yields a set of integrated intensities $I_H(\psi)$, which – in the homogeneous case – contains the texture distribution $T_H(\psi)$. The $T_H(\psi)$ distribution accounts for the volume density of lattice planes (*HKL*) at inclination angle ψ and has to be used in a normalized form in order to cover all crystallites in the sample. Describing for instance the texture distribution by the shape of the $\cos^n\psi$ function, a normalization factor of $(n+1)/2\pi$ has to be chosen. The distribution is characterized by the convenient property that the concentration of lattice planes in the fiber pole – usually given in (intensity) multiples of a random distribution or m.r.d. – directly scales with the order parameter n.
The combined effect of attenuation of the incoming X-ray and tilting of the sample is described by the configuration factor $k = 2/(\sin\theta\cos\psi)$, the product of which with μ has the meaning of an inverse penetration depth. In our approach, distinct $I_H(\psi)$ distributions are measured for different wavelengths λ. The basic principle is sketched in figure 1(b), where the damping of intensity $I/I_0 = \exp(-\mu tk)$ is shown for the ZnO 002 Bragg peak at $\psi = 0°$ and 60° for two different beam energies of 8 and 10 keV. The abscissa is given in units of μt for a thin ZnO:Al film having $\mu t = 0.0113$ and 0.0449 at both energies. It is the difference between the branches of this plot, from which the information on texture gradation is deduced or any other microstructure gradient may be derived.

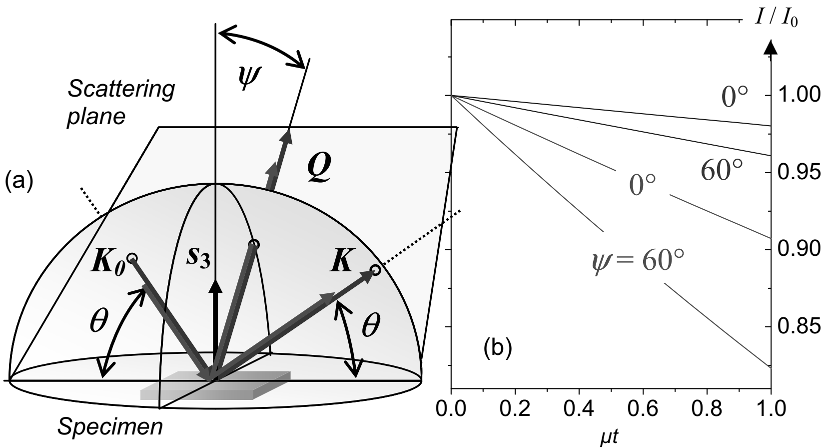

Figure 1. (a) Experimental set-up for θ-2θ measurements under various tilt angles and for different wavelengths, with the latter being symbolized by incoming and exiting wave vectors $\boldsymbol{K_0}$ and $\boldsymbol{K}$ of different color and magnitude. For non zero tilts, $\psi \neq 0$, the scattering vector $\boldsymbol{Q} = \boldsymbol{K} - \boldsymbol{K_0}$ deviates from the direction of the substrate normal $\boldsymbol{s}_3$. (b) Damping of intensity I/I_0 in fiber texture measurements of 002 Bragg reflection from thin ZnO:Al films with two different X-ray energies of 8 and 10 keV (solid and dashed line). I/I_0 values are plotted versus μt and for two tilt angle positions.

Techniques for analyzing non-homogeneous textures in the framework of the kinematic theory were recently put forward [7, 36]. If graded fiber textures are considered, a depth-

dependent distribution function $T_H(\psi, z)$ has to be introduced. It has been shown that the kinematical intensity of the fiber peak can be described by the finite Laplace transform [37] of the texture distribution $\mathcal{L}^t(T_H)$ [36], where the transformation is from z space to the penetration depth coordinate $(\mu k)^{-1}$. The general expression for the Bragg peak intensity becomes

$$I_H(\psi,t) = SCF\,\lambda^3\,Lp\left|F_H\right|^2 m_H \frac{k}{2}\mathcal{L}^t(T_H). \tag{1}$$

In this expression SCF, Lp, F_H and m_H stand for an instrumental scaling factor, Lorentz-polarization and structure factor and the multiplicity of the reflection.
For $T_H = ((n+1)/2\pi)\cos^n\psi$ model functions the depth dependence might be included by interpreting the texture order n as a z-dependent polynomial. Analytical solutions of (1) are possible by restricting the polynomial degree to the most simple case, i.e. by setting $n = n_0 + n_1 z$. In passing we note that the fiber texture gradient n_1 is of dimensionality m.r.d. per unit depth. Interpreting n_0 and n_1 in terms of figure 1(b) it means that the single parameter n_0 of the ungraded cases could be deduced from either the difference between the two upper or two lower curves. Intending, moreover, to determine both n_0 and n_1, at least two $I_H(\psi)$ distributions have to be measured at different wavelengths. In case of a linear z dependence of n the finite Laplace transform is solved to yield

$$\frac{k}{2}\mathcal{L}^t(T_H) = \widetilde{N}\cos^{n_0}\psi\,\frac{k}{2M}\widetilde{A}(t), \tag{2}$$

where $M = \mu k - n_1\ln(\cos\psi)$ is valid, with Mt now replacing the μtk product, the latter being significant only in the gradient-free texture case. In addition, the abbreviations

$$\widetilde{A}(t) = 1-\exp(-Mt) = 1-(\cos^{n_1 t}\psi)\exp(-\mu tk), \tag{3}$$

$$\widetilde{N} = \frac{1}{2\pi}\left[n_0 + n_1 t\left(\frac{1}{Mt}+\frac{1}{1-e^{Mt}}\right)+1\right] \tag{4}$$

are used in equation (2) that stand for the generalized absorption factor and generalized normalization factor in the graded texture case [36]. It has to be emphasized that the fiber texture gradient n_1 appears as the product $n_1 t$ and it is this quantity that may be derived from the analysis.

3. Experimental

Layers of ZnO:Al were prepared by reactive magnetron sputtering from a Zn-2wt%Al alloy target, for further details see Refs. [29, 30]. Highly accurate μt products of these samples were derived from atomic area densities Nt determined by Rutherford backscattering [30], applying the connection of both quantities through the molecular weight M_W and mass attenuation coefficient μ_m via $\mu t = \mu_m M_W Nt$. This calculation also allowed for the determination the projected thickness $t_{pro} = \mu t/(\rho\mu_m)$ that is understood as the thickness the layer would have in case its density would compare to the bulk value ρ [8] (in general, the effective thickness of a thin film exceeds the projected one due to inclusion of voids and other excess volume). t_{pro} values of the investigated samples amounted to 118 nm, 246 nm and 413 nm.
Diffraction experiments were performed at BESSY II bending magnet beam line KMC-2 operating with a graded-SiGe/SiGe double-crystal monochromator to achieve an energy resolution $\Delta E/E$ of about 10^{-4} [38]. A six-circle goniometer and a scintillation counter were

used for the measurement with beam energies set to 8.048 and 10 keV (abbreviated by 8 and 10 keV in the following). This choice of X-ray energies was motivated, firstly, to allow for comparison of one set of results with those from laboratory experiments by employing a conventional copper tube. Secondly, the higher beam energy is sufficiently above the Zn *K* edge to ensure that EXAFS oscillation in the mass attenuation coefficient μ_m are damped out [39] and to validate the use of the free atom value. Since highly precise intensity values were required for the modeling of equation (1) the experiments were set out to measure only few reflections with a high peak-to-background ratio.

Intensity $\theta/2\theta$ scans of 002 Bragg peaks were collected from each sample for both energies, while inclinations ψ were adjusted to 0, 10, 20, 30, 45 and 60°. Measured intensity data were corrected for peak asymmetry introduced by the Lorentz-polarization factor, which was applied in the appropriate form for in-plane polarized synchrotron radiation, $Lp = (\sin\theta \sin 2\theta)^{-1}$. Lp-corrected Bragg peaks were fitted by pseudo Voigt function profiles yielding the desired integral intensity distributions $I_H(\psi)/Lp$ with estimated standard deviations on the order of 1..2% for maximum intensities at $\psi = 0$.

The results are displayed in figure 2 for the thickest sample with error bars comparable to the size of the dots. Those values were subsequently divided by $\lambda^3 |F_H|^2 m_H$ and subjected to a non-linear regression in terms of equation (1) and (2). Effects due to the polar space group of ZnO were estimated to be of minor significance and were thus neglected by usage of an averaged structure factor F_H. Normal and anomalous scattering factors *f*, *f'*, *f"* as well as mass attenuation coefficients μ_m for both X-ray wavelengths were consistently taken from the Berkeley X-ray server [40], see table 1. Unit cell parameters *a*, *c* and oxygen positional parameter *u* were from Abrahams and Bernstein [41].

Table 1. Normal and anomalous scattering factors f, f' and f" and mass attenuation coefficients μ_m of the three elements contained in the samples; f values are specified for the 002 peak position at $\sin\theta/\lambda = 1.92$ nm^{-1}. All data according to [40].

		8 keV			10 keV		
	f	***f'***	***f"***	μ_m (cm^2 g^{-1})	***f'***	***f"***	μ_m (cm^2 g^{-1})
Zn	24.56	-1.56	0.7035	56.35	-2.69	3.694	237.9
O	5.768	0.0522	0.0337	11.13	0.036	0.021	5.673
Al				46.88			24.76

4. Results and discussion

The regression of corrected intensities $I_H(\psi)/(\lambda^3 Lp |F_H|^2 m_H)$ was performed for each sample to both energies simultaneously by assuming n_0 and $n_1 t$ to be independent of energy. Only the scaling factors decomposed into distinct values SCF(E_1) and SCF(E_2). The resulting fitting curve is also presented in figure 2. It is realized from this plot that an excellent agreement of the measured distributions was achieved by modeling the fiber texture gradient with equations (1) to (4).

The values obtained by the regression for n_0 and $n_1 t$ are given in figure 3 as a function of sample thickness. It is realized from this figure that $n_1 t$ shows a falling tendency, while the opposite trend is observed for n_0. This reflects an increase of preferred orientation with increasing thickness of ZnO:Al layers, albeit the grading of texture is diminishing. Both results are fully in accordance with previous studies [29] justifying the reliability of the approach. The inset of the figure depicts the course of n_1, the values of which were derived from the $n_1 t/t_{pro}$ ratio. For the thinnest sample, having t_{pro} = 118 nm, the texture gradient n_1 approaches a value of 0.3 m.r.d. nm^{-1} averaged over the full depth of the layer, which means that every three nanometers the texture order n increases by one m.r.d. unit.

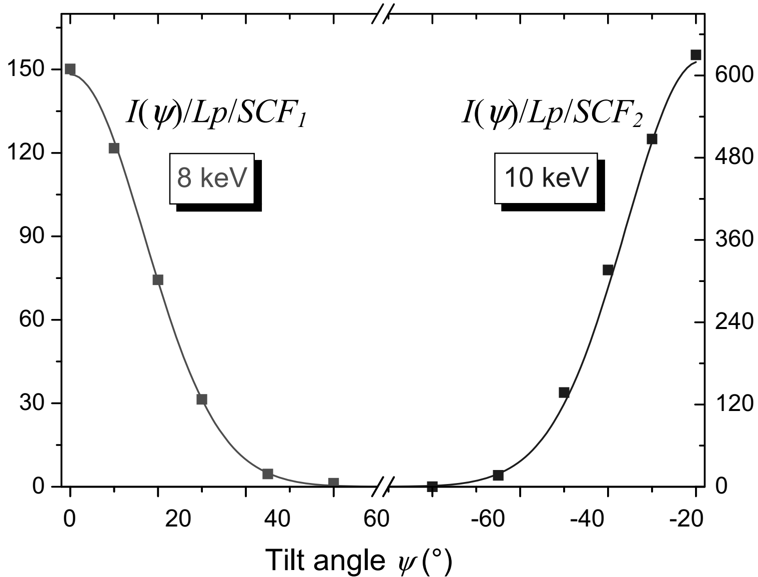

Figure 2. Experimental results of measured $I_H(\psi)/Lp$ values (black dots) and model curve (continuous line) with n_0 and $n_1 t$ values given in figure 3. Experimental data and model curve were both divided by the instrumental scaling factor SCF derived from the fit.

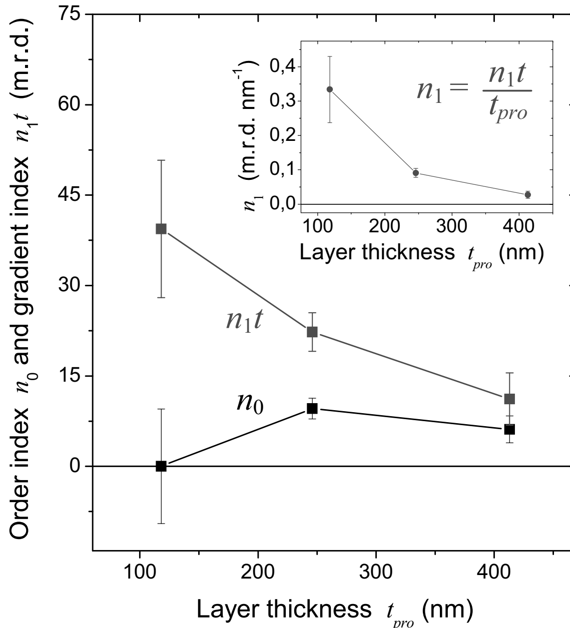

Figure 3. Quantitative results and estimated standard deviations for the initial texture index n_0 and the product of thickness and texture gradient n_1t for the investigated samples. The inset shows the pure texture gradient n_1 in units of m.r.d. nm^{-1}.

This unexpected and remarkably large value underlines the strong increase of fiber texture with increasing thickness in these samples. It indicates strong re-ordering processes to occur on an atomic scale within already deposited layers that might either be due to bulk diffusion or plastic deformation processes.

The results also show that the strongest texture gradient is observed close to the layer-substrate interface. This contrasts to the gradients typically encountered for residual stress, where the strongest variations are mostly observed in the vicinity of the layer surface. An on-going discussion is concerned with the relation between fiber texture and residual stress evolution and whether one could be the cause of the other microstructural property [11, 16, 17, 20, 22-24, 26].

Apparently, this discussion will benefit from the availability of quantitative results of fiber texture gradients as they may be determined by the formalism presented in this work. It may be expected that future investigations of combined texture, residual stress and other microstructure gradients will yield a more comprehensive picture of individual thin film growth processes. With the introduction of the technique for evaluating fiber texture gradients as presented in this work a further tool for this long-term task has been provided.

5. Conclusions

The quantitative determination of fiber texture gradients has successfully been performed for the example of thin polycrystalline films. The presented technique may be applied to a single thin film specimen and lifts the burden of preparing complete sample series of different thickness or to rely on *in-situ* XRD techniques. To the best of our knowledge this is the first work, where a fiber texture gradient has been determined quantitatively in the appropriate dimensions of multiples of a random distribution per unit depth. Large texture gradients on the order of 0.03 to 0.3 m.r.d. nm^{-1} have been uncovered for thin ZnO:Al films, with the strongest texture increase occurring close to the interface to the substrate. The presented concept is completely general and may equally be applied to other material systems and other orientation distributions than of the $\cos^n \psi$ type. It can be expected that the quantitative determination of texture gradients will deliver valuable experimental input to extend the spare data base of microstructure gradients as required for a perspective full theoretical modeling of thin film growth.

References

1. Movchan, B.A. & Demchishin, A.V., 1969, *Phys. Met. Metallogr.*, **28**, 83.
2. Thornton, J.A., 1974, *J. Vac. Sci. Tech.*, **11**, 666.
3. Machlin, E.S., 1995. *The Relationship between Thin Film Processing and Structure*. Materials Science in Microelectronics (Croton-on-Hudson: Giro Press).
4. Bunge, H.-J., 1982. *Texture Analysis in Materials Science* (London: Butterworth).
5. Wenk, H.-R. & van Houtte, P., 2004, *Rep. Prog. Phys.*, **67**, 1367.
6. Bonarski, J.T., Bunge, H.J., Wcislak, L. & Pawlik, K., 1998, *Textures Microstruc.*, **31**, 21.
7. Bonarski, J.T., 2006, *Prog. Mat. Sc.*, **51**, 61.
8. Birkholz, M., 2006. *Thin Film Analysis by X-ray Scattering* (Weinheim: Wiley-VCH), chapter 5 and pp 64-66.
9. Harper, J.M.E., Cabral, C., Andricacos, P.C., Gignac, L., Noyan, I.C., Rodbell, K.P. & Hu, C.K., 1999, *J. Appl. Phys.*, **86**, 2516.
10. Okolo, B., Lamparter, P., Welzel, U. & Mittemeijer, E.J., 2004, *J. Appl. Phys.*, **95**, 466.
11. Birkholz, M., Genzel, C. & Jung, T., 2004, *J. Appl. Phys.*, **96**, 7202.
12. Birkholz, M., Selle, B., Conrad, E., Lips, K. & Fuhs, W., 2000, *J. Appl. Phys.*, **88**, 4376.
13. Birkholz, M., Conrad, E. & Fuhs, W., 2001, *Jpn. J. Appl. Phys.*, **40**, 4176
14. Reinig, P., Fenske, F., Fuhs, W., Alex, V. & Birkholz, M., 2002, *J. Vac. Sc. Technol. A*, **20**, 2004.
15. Morales, M., Leconte, Y., Rizk, R. & Chateigner, D., 2004, *J. Appl. Phys.*, **97**, 034307.
16. Pelleg, J., Zevin, L.Z., Lungo, S. & Croitoru, N., 1991, *Thin Solid Films*, **197**, 117.
17. Oh, U.C. & Je, J.H., 1993, *J. Appl. Phys.*, **74**, 1692.

18. Knuyt, G., Quaeyhaegens, C., D'Haen, J. & Stals, L.M., 1995, *Thin Solid Films*, **258**, 159.
19. Quaeyhaegens, C., Knuyt, G., D'Haen, J. & Stals, L.M., 1995, *Thin Solid Films*, **258**, 170.
20. Greene, J.E., Sundgren, J.-E., Hultman, L., Petrov, I. & Bergstrom, D.B., 1995, *Appl. Phys. Lett.*, **67**, 2928.
21. Sloof, W.G., Kooi, B.J., Delhez, R., de Keijser, T.H. & Mittemeijer, E.J., 1996, *J. Mater. Res.*, **11**, 1440.
22. Genzel, C. & Reimers, W., 1998, *phys. stat. sol. (a)*, **166**, 751.
23. Leoni, M., Scardi, P., Rossi, S., Fedrizzi, L. & Massiani, Y., 1999, *Thin Sol. Films*, **345**, 263.
24. Rauschenbach, B. & Gerlach, J.W., 2000, *Cryst. Res. Technol.*, **35**, 675.
25. Schell, N., Bottiger, J., Matz, W. & Chevallier, J., 2003, *Nucl. Instr. Meth.*, **B 199**, 133.
26. Abadias, G. & Tse, Y.Y., 2004, *J. Appl. Phys.*, **95**, 2414.
27. Fujimura, N., Nishihara, T., Goto, S., Xu, J. & Ito, T., 1993, *J. Cryst. Growth*, **130**, 269.
28. Jiang, X., Jia, C.L. & Szyska, B., 2002, *Appl. Phys. Lett.*, **80**, 3090.
29. Birkholz, M., Selle, B., Fenske, F. & Fuhs, W., 2003, *Phys. Rev. B*, **68**, 205414.
30. Fenske, F., Selle, B. & Birkholz, M., 2005, *Jpn. J. Appl. Phys.*, **44**, L662.
31. Berdahl, P., Reade, R.P., Liu, J., Russo, R.E., Fritzemeier, L., Buczek, D. & Schopp, U., 2003, *Appl. Phys. Lett.*, **82**, 343.
32. Ricote, J., Poyato, R., Alguero, M., Pardo, L., Calzada, M.L. & Chateigner, D., 2003, *J. Am. Ceram. Soc.*, **86**, 1571.
33. van der Drift, A., 1967, *Philips Res. Rep.*, **22**, 267.
34. Bradley, R.M., Harper, J.M.E. & Smith, D.A., 1986, *J. Appl. Phys.*, **60**, 4160.
35. Rauschenbach, B. & Helming, K., 1989, *Nucl. Instr. Meth.*, **B42**, 216.
36. Birkholz, M., 2007, *J. Appl. Cryst.*, **40**, 735.
37. Doetsch, G., 1970. *Einführung in die Theorie und Anwendung der Laplace-Transformation* (Basel: Birkenhäuser).
38. Erko, A., Packe, I., Gudat, W., Abrosimov, N. & Firsov, A., 2000, *A Graded Crystal Monochromator at BESSY II*, in *SPIE conf. proc.* **4145**, edited by A.K. Freund et al., p. 122.
39. Decremps, F., Datchi, F., Saitta, A.M., Polian, A., Pascarelli, S., Di Cicco, A., Itié, J.P. & Baudelet, F., 2003, *Phys. Rev. B*, **68**, 104101.
40. Henke, B.L., Gullikson, E.M. & Davis, J.C., 1993, *Atomic Data Nucl. Data Tab.*, **54**, 181.
41. Abrahams, S.C. & Bernstein, J.L., 1969, *Acta Cryst.*, **B25**, 1233.

Acknowledgements. We thank Daniel Chateigner, Christoph Genzel, Maarten Heyn, Peter Zaumseil and Harald Beyer for helpful discussion and Frank Fenske for leaving these otherwise already fruitful samples for this investigation.